Neutron Electric Dipole Moment and Tensor Charges from Lattice QCD

Tanmoy Bhattacharya,[1, *] Vincenzo Cirigliano,[1, †] Rajan Gupta,[1, ‡] Huey-Wen Lin,[2, §] and Boram Yoon[1, ¶]

(Precision Neutron-Decay Matrix Elements (PNDME) Collaboration)

[1]*Los Alamos National Laboratory, Theoretical Division T-2, Los Alamos, NM 87545*
[2]*Physics Department, University of California, Berkeley, CA 94720*
(Dated: January 11, 2016)

We present lattice QCD results on the neutron tensor charges including, for the first time, a simultaneous extrapolation in the lattice spacing, volume, and light quark masses to the physical point in the continuum limit. We find that the "disconnected" contribution is smaller than the statistical error in the "connected" contribution. Our estimates in the $\overline{\text{MS}}$ scheme at $2\,\text{GeV}$, including all systematics, are $g_T^{d-u} = 1.020(76)$, $g_T^d = 0.774(66)$, $g_T^u = -0.233(28)$, and $g_T^s = 0.008(9)$. The flavor diagonal charges determine the size of the neutron electric dipole moment (EDM) induced by quark EDMs that are generated in many new scenarios of CP-violation beyond the Standard Model (BSM). We use our results to derive model-independent bounds on the EDMs of light quarks and update the EDM phenomenology in split supersymmetry with gaugino mass unification, finding a stringent upper bound of $d_n < 4 \times 10^{-28}\,e$ cm for the neutron EDM in this scenario.

Low-energy precision measurements of neutron properties provide unique probes of new physics at the TeV scale. Searches for the neutron permanent EDM d_n have high sensitivity to new beyond the standard model (BSM) CP-violating interactions. Similarly, precision studies of correlations in neutron decay are sensitive to possible BSM scalar and tensor interactions. To fully realize the potential of the vibrant existing experimental neutron physics program [1], one needs to accurately calculate matrix elements of appropriate low-energy effective operators within neutron states. In this paper we describe lattice QCD calculations of the neutron tensor charges. In the future, these charges will be extracted with competitive precision from various measurements of the quark transversity distributions at JLab [2], and provide robust tests of the lattice results.

The flavor diagonal charges $g_T^{u,d,s}$ are needed to quantify the contribution of the quark EDM to the neutron EDM and thus set bounds on BSM sources of CP violation. We find that the contribution of the "disconnected" diagrams to g_T^u, g_T^d and g_T^s are small. Our results on these charges allow us to constrain split supersymmetry models.

The isovector charge g_T^{d-u} is needed in the analysis of precision neutron β-decay. In Ref. [3] we showed that to complement experimental measurements of the helicity flip contributions to neutron β-decay at the precision of planned experiments (10^{-3} level), we need to calculate the iso-vector scalar and tensor charges, g_S^{d-u} and g_T^{d-u}, to about 10% accuracy. Results for g_T^{d-u} presented here meet the desired accuracy with control over all systematic errors, while g_S^{d-u} requires $O(10)$ more statistics.

Details of the lattice QCD calculations are given in a companion paper [4]. Here we summarize the main points and focus on the results using nine ensembles of $N_f = 2 + 1 + 1$ flavors of highly improved staggered quarks (HISQ) [5] generated by the MILC Collaboration [6] and described in Table I. On these ensembles, we construct correlation functions using Wilson-clover fermions, as these preserve the continuum spin structure. To reduce short-distance noise, all lattices were "HYP" smeared [7]. Extensive tests were carried out on these nine HYP smeared ensembles to look for the presence of exceptional configurations [8], a possible problem with this mixed-action, clover-on-HISQ, approach. None were detected. Issues of statistics, excited state contamination, operator renormalization, lattice volume, lattice spacing and the chiral behavior are detailed in [4].

The flavor diagonal neutron charges g_Γ^q are defined by $\langle n(p,s)|\mathcal{O}_\Gamma^q|n(p,s)\rangle = g_\Gamma^q \bar{u}_s(p)\Gamma u_s(p)$, with $O_\Gamma^q = \bar{q}\Gamma q$ and the spinors satisfying $\sum_s u_s(\mathbf{p})\bar{u}_s(\mathbf{p}) = (\not{p} + m)$. The interpolating operator we use to create/annihilate the relativistically normalized neutron state $|n(p,s)\rangle$ is $\chi(x) = \epsilon^{abc} \left[q_1^{aT}(x) C \gamma_5 \frac{1}{2}(1+\gamma_4) q_2^b(x) \right] q_1^c(x)$ with color indices $\{a, b, c\}$, charge conjugation matrix C, and q_1, q_2 the two different flavors of light quark fields.

The zero-momentum projection of $\chi(x)$ couples to the ground state, all radially excited states of the neutron, and multiparticle states. To reduce the coupling to radially excited states we Gaussian smear the quark fields in $\chi(x)$. To isolate the remaining excited state contamination, we include two states in the analysis of the two- and three-point functions at zero momentum [4]. Even though the excited state contribution is exponentially suppressed, we were able to isolate the leading two unwanted matrix elements $\langle 0|\mathcal{O}_\Gamma|1\rangle$ and $\langle 1|\mathcal{O}_\Gamma|1\rangle$, where $|0\rangle$ and $|1\rangle$ represent the ground and first excited neutron states. We find that the magnitude of $\langle 0|\mathcal{O}_\Gamma|1\rangle$ is about 16% of $\langle 0|\mathcal{O}_\Gamma|0\rangle$ and is determined with about 20% uncertainty on all the ensembles, whereas

Ensemble ID		a (fm)	M_π^{sea} (MeV)	M_π (MeV)	$L^3 \times T$	$M_\pi L$	t_{sep}/a	N_{conf}	N_{meas}
a12m310	△	0.1207(11)	305.3(4)	310.2(2.8)	$24^3 \times 64$	4.55	$\{8, 9, 10, 11, 12\}$	1013	8104
a12m220S	◁	0.1202(12)	218.1(4)	225.0(2.3)	$24^3 \times 64$	3.29	$\{8, 10, 12\}$	1000	24000
a12m220	▷	0.1184(10)	216.9(2)	227.9(1.9)	$32^3 \times 64$	4.38	$\{8, 10, 12\}$	958	7664
a12m220L	▽	0.1189(09)	217.0(2)	227.6(1.7)	$40^3 \times 64$	5.49	10	1010	8080
a09m310	✧	0.0888(08)	312.7(6)	313.0(2.8)	$32^3 \times 96$	4.51	$\{10, 12, 14\}$	881	7048
a09m220	✩	0.0872(07)	220.3(2)	225.9(1.8)	$48^3 \times 96$	4.79	$\{10, 12, 14\}$	890	7120
a09m130	✿	0.0871(06)	128.2(1)	138.1(1.0)	$64^3 \times 96$	3.90	$\{10, 12, 14\}$	883	7064
a06m310	□	0.0582(04)	319.3(5)	319.6(2.2)	$48^3 \times 144$	4.52	$\{16, 20, 22, 24\}$	1000	8000
a06m220	◇	0.0578(04)	229.2(4)	235.2(1.7)	$64^3 \times 144$	4.41	$\{16, 20, 22, 24\}$	650	2600

TABLE I. The parameters of the (2+1+1) flavor HISQ lattices are quoted from Ref. [6]. The symbols used in the plots are defined along with the ensemble ID. All chiral analyses are carried out with respect to the clover valence pion masses M_π which are tuned to be close to the Goldstone HISQ pion masses M_π^{sea}. We also give the source-sink separations (t_{sep}/a) simulated, configuration analyzed (N_{conf}) and the total number of measurements (N_{meas}) made. Finite volume analysis is done in terms of $M_\pi L$.

$|\langle 1|\mathcal{O}_\Gamma|1\rangle| \sim \langle 0|\mathcal{O}_\Gamma|0\rangle$, but has $O(100\%)$ errors. As illustrated in Fig. 1 for the *a09m310* ensemble, the overlap of data in the center of the fit range for all the source-sink separations t_{sep} indicates that excited state contamination in the tensor charges is small and under control.

The disconnected diagrams are estimated using a stochastic method accelerated with a combination of the truncated solver method (TSM) [9, 10], the hopping parameter expansion (HPE) [11, 12] and the all-mode-averaging (AMA) technique [13]. In most cases, the disconnected contribution is small and consistent with zero as illustrated in Fig. 1 for the *a09m310* ensemble. This feature was also observed in Ref. [14]. We find that the light quark contribution is too noisy to extrapolate to the continuum limit, so we do not include it in the central value. We, however, use the largest estimate, 0.0121, on the coarsest ensemble *a12m310* as an additional systematic error in g_T^d, g_T^u, and g_T^{d+u}.

The renormalization factor, calculated nonperturbatively in the RI-sMOM scheme [15, 16] using the isovector operator, contributes a significant fraction of the total error. The charges converted into the $\overline{\mathrm{MS}}$ scheme at $2\,\mathrm{GeV}$ are given in Table II and Fig. 2. They are essentially flat in the three variables, lattice spacing a, the pion mass M_π and the spatial lattice size L. We make a simultaneous fit to the data using the lowest order ansatz appropriate to our not fully $O(a)$ improved clover-on-HISQ formulation:

$$g_T(a, M_\pi, L) = c_1 + c_2 a + c_3 M_\pi^2 + c_4 e^{-M_\pi L}. \quad (1)$$

As discussed in [4], with current data the extrapolation to the physical point ($M_\pi = 135$ MeV, $a = 0$, $M_\pi L = \infty$) is insensitive to additional corrections. The final renormalized charges for the neutron [17] are

$$g_T^d = 0.774(66), \qquad g_T^u = -0.233(28),$$
$$g_T^{d-u} = 1.020(76), \qquad g_T^{d+u} = 0.541(67). \quad (2)$$

The χ^2/dof for the fits are 0.1, 1.6, 0.4 and 0.2, respectively, with dof = 5. Including the leading chiral loga-

rithms [18] in Eq. (1) gives similar results [4]. g_T^s, after extrapolation in the lattice spacing a and M_π^2, is

$$g_T^s = 0.008(9), \quad (3)$$

with a $\chi^2/\mathrm{dof} = 0.29$ with dof = 2. The intercept of the fit on the $[g_T^s, a]$ plane is shown in Fig. 3.

Our result for g_T^{d-u}, with control over all systematic errors, is in good agreement with other lattice calculations [19, 20]. The LHPC [21] and RQCD [22] Collaborations also find no significant dependence on the lattice spacing and volume, but do find a small dependence on the quark mass, so they extrapolate only in the quark mass using linear/quadratic (LHPC) and linear (RQCD) fits in M_π^2. Their final estimates, $g_T^{d-u} = 1.038(11)(12)$ (LHPC) and $g_T^{d-u} = 1.005(17)(29)$ (RQCD) are consistent with ours. A fit to our data versus only M_π^2, shown as an overlay in Fig. 2 (center), gives a similarly accurate estimate $g_T^{d-u} = 1.059(29)$ with a $\chi^2/\mathrm{dof} = 0.3$.

Our results on the tensor charges have implications for the neutron EDM and CP-violation in BSM theories. At the hadronic scale, $\mu \sim O(1)$ GeV, after integrating out all heavy degrees of freedom the dominant effect of new CP-violating couplings in BSM theories is encoded in local operators of dimension five and six. Leading, among them, are the elementary fermion EDMs [23, 24]:

$$\delta\mathcal{L}_{\mathrm{CPV}} \supset -\frac{ie}{2} \sum_{f=u,d,s,e} d_f \, \bar{f}\sigma_{\mu\nu}\gamma_5 F^{\mu\nu} f. \quad (4)$$

The contribution of the quark EDM d_q to d_n is [25, 26]

$$d_n = g_T^u \, d_u + g_T^d \, d_d + g_T^s \, d_s, \quad (5)$$

consequently, improved knowledge of g_T^q combined with experimental bounds on d_n provides stringent constraints on new CP violation encoded in d_q.

Our calculation has the following impact: (i) We reduce the uncertainty on $g_T^{u,d}$ from the $\sim 50\%$ of previous QCD sum rules (QCDSR) estimates [27] to the 10%
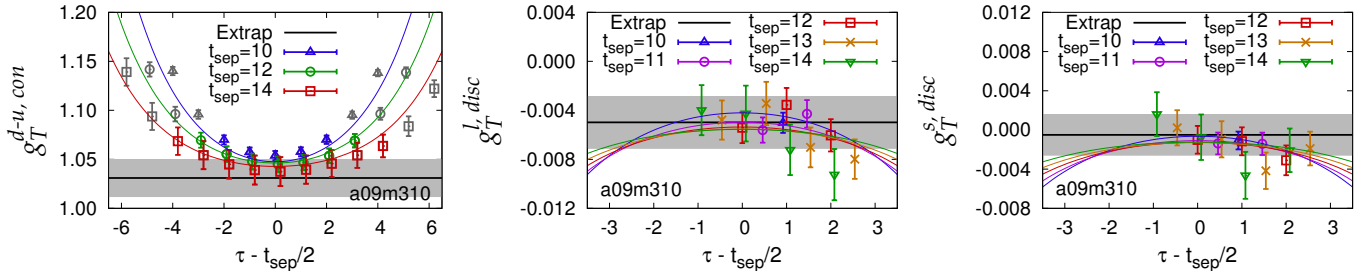
FIG. 1. Fits illustrating the excited state contribution in the connected g_T^{d-u} and light and strange disconnected diagram for the $a09m310$ ensemble. The data points represent $g_T^q(\tau, t_{\rm sep})$ obtained from calculations at different source-sink separations $t_{\rm sep}$ and operator insertion times τ. The solid black line and the gray band are the ground state estimate and error.
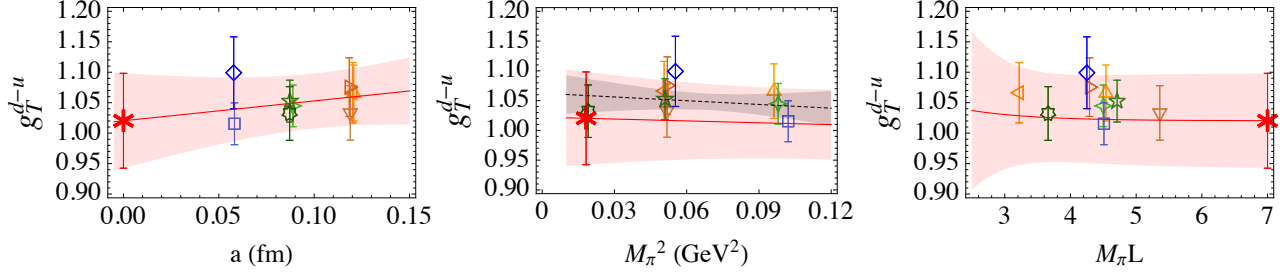

FIG. 2. A simultaneous fit of neutron g_T^{d-u} data versus a, M_π^2, and $M_\pi L$ using Eq. (1). The error band is shown as a function of each variable holding the other two at their physical value. The data are shown projected on to each of the three planes. The symbols are defined in Table I. The extrapolated value is marked by a red star. The thin gray band and the dashed line within it in the middle panel show the fit versus M_π^2 assuming no dependence on the other two variables.
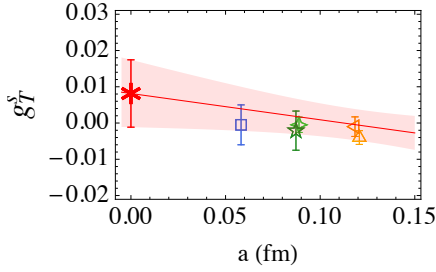

FIG. 3. The data for g_T^s and intercept of the fit versus a and M_π on the $[g_T^s, a]$ plane. Notation is the same as in Fig. 2.
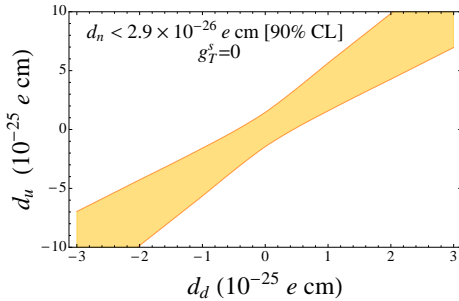

FIG. 4. Bounds on $d_{u,d}$, defined in the $\overline{\rm MS}$ scheme at 2 GeV, with a 1σ slab prior on g_T^u and g_T^d given in Eq. (2) and $g_T^s = 0$.

FIG. 5. Iso-level lines of d_n and d_e in split SUSY in the M_2-μ plane using $\sin\phi = 1$, $\tan\beta = 1$, and central values of $g_T^{u,d,s}$.

level. (For a comparison of the lattice results with the Dyson-Schwinger [28] and other methods [29–32] see [4].) (ii) The central values of $g_T^{u,d}$ are roughly 3/5 of the QCDSR and quark mod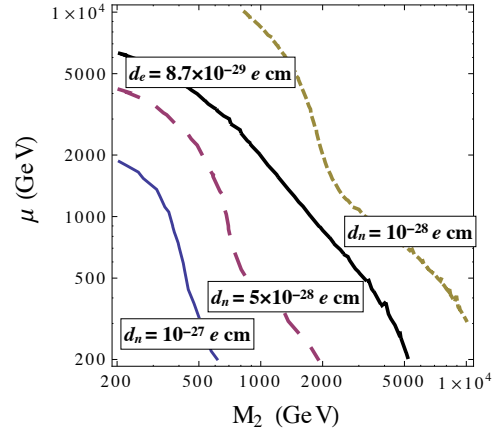el estimates [27] widely used in phenomenological studies of BSM CP violation. (iii) Bounding the strangeness tensor charge g_T^s at the percent level is important for a large class of models in which $d_q \propto m_q$ since $m_s/m_d \sim 20$. Our results imply that in such models $g_T^s d_s$ may contribute up to 35% of the total d_n and the current $O(1)$ fractional uncertainty in g_T^s gives rise to the largest uncertainty in d_n. The contribution of EDMs of heavier quarks to nEDM appears at two-loops and does not grow with m_q. In this work, we ignore contributions of the charm (not calculated) and heavier quarks.

Ensemble ID	$g_T^{\mathrm{con},d}$	$g_T^{\mathrm{con},u}$	$g_T^{\mathrm{con},d-u}$	$g_T^{\mathrm{con},d+u}$	$g_T^{\mathrm{disc},l}$	$g_T^{\mathrm{disc},s}$
a12m310	0.852(37)	−0.215(12)	1.066(46)	0.637(31)	−0.0121(23)	−0.0040(19)
a12m220S	0.857(43)	−0.209(19)	1.066(50)	0.649(44)	—	—
a12m220	0.860(40)	−0.215(15)	1.075(48)	0.644(36)	−0.0037(40)	−0.0010(27)
a12m220L	0.840(37)	−0.194(12)	1.033(45)	0.647(33)	—	—
a09m310	0.840(28)	−0.2051(98)	1.045(34)	0.634(25)	−0.0050(22)	−0.0005(21)
a09m220	0.836(28)	−0.216(10)	1.053(34)	0.619(25)	—	−0.0021(54)
a09m130	0.809(40)	−0.222(20)	1.032(44)	0.587(45)	—	—
a06m310	0.815(29)	−0.199(10)	1.015(34)	0.617(27)	−0.0037(65)	−0.0005(55)
a06m220	0.833(52)	−0.264(22)	1.099(59)	0.569(55)	—	—

TABLE II. Renormalized estimates of the connected (g_T^{con}) and disconnected (g_T^{disc}) contributions in the $\overline{\mathrm{MS}}$ scheme at 2 GeV.

While, in general, BSM theories generate additional CP-violating operators in Eq. (4), there exist models in which the fermion EDMs are the dominant sources of CP violation at low-energy, thus controlling the pattern of hadronic and atomic EDMs. For such cases, using Eq. (5), our results on the tensor charges, and the experimental limit on the neutron EDM [33], we show 90% confidence level (CL) bounds on quark EDMs $d_{u,d}$ in Fig. 4 [34].

One notable scenario in which fermion EDM operators provide the dominant BSM source of CP violation is "split SUSY" [35–37], in which all scalars, except for one Higgs doublet, are much heavier than the electroweak scale. This SUSY scenario achieves gauge coupling unification, has a dark matter candidate, and avoids the most stringent constraints associated with flavor and CP observables mediated by one-loop diagrams involving scalar particles. Contributions to fermion EDMs arise at two loops due to CP violating phases in the gaugino-Higgsino sector, while all other operators are highly suppressed [38, 39]. To illustrate the impact of improved estimates of matrix elements in split SUSY, we use the analytic results and setup of Ref. [38], namely unified framework for gaugino masses at the GUT scale and a scalar mass $\tilde{m} = 10^9$ GeV. The light fermion EDMs $d_{e,u,d,s}$ depend on a single phase ϕ, on $\tan\beta$ [approximately through the overall factor $\sin(\phi)\sin(2\beta)$] and on the gaugino (M_2) and Higgsino (μ) mass parameters. Following Ref. [38] we set $\tan\beta = 1$, $\sin\phi = 1$ and present the results as contours in the M_2-μ plane, in the range between 200 GeV and 10 TeV.

Figure 5 shows iso-level curves of d_n as well as the curve $d_e = 8.7 \times 10^{-29} e$ cm, corresponding to the current 90% C.L. limit [40]. For the neutron EDM we use Eq. (5), evaluating both the d_q's and the tensor charges at the scale $\mu^{\overline{\mathrm{MS}}} = 2$ GeV. Our result for d_n is appreciably smaller (factor of ~ 3) than the one in Ref. [38]. We have traced back this difference to (i) our smaller values of the tensor charges compared to QCDSR [27]; (ii) different values for the light quark masses: we use the PDG [41] central value $m_d(\overline{\mathrm{MS}}, \mu = 2\mathrm{GeV}) = 4.75$ MeV, while the value corresponding to the quark condensate
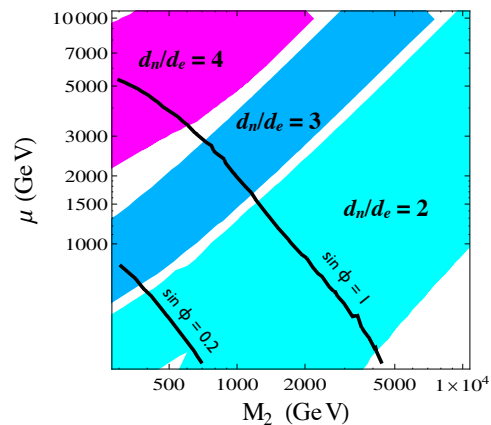

FIG. 6. Regions in M_2-μ plane corresponding to $d_n/d_e = 2, 3, 4$ in split SUSY, obtained by varying $g_T^{u,d,s}$ within our estimated uncertainties. The lines correspond to $d_e = 8.7 \times 10^{-29} e$ cm for $\sin\phi = 0.2, 1$.

used in Ref. [38] is larger, $m_d(\overline{\mathrm{MS}}, \mu = 1\mathrm{GeV}) \approx 9$ MeV.

In Refs. [38, 42], it was pointed out that the strong correlation between electron and neutron EDM would provide a valuable experimental test of split SUSY. To investigate this further, in Fig. 6 we present bands corresponding to different values of d_n/d_e in the M_2-μ plane, the thickness of the bands reflects the behavior of $d_n/d_e[M_2, \mu]$ and the uncertainty induced by the tensor charges, dominated by g_T^s. The fact that we can draw disconnected bands for $d_n/d_e = 2, 3, 4$ is a welcome consequence of our reduced uncertainties in g_T^q: using the QCDSR input, each band would be as thick as the whole plot, giving essentially no discrimination.

Finally, based on the current 90% C.L. limit on d_e, we derive an upper limit for the neutron EDM in split SUSY. By maximizing the ratio d_n/d_e along the iso-level curves $d_e = 8.7 \times 10^{-29} e$ cm corresponding to $\sin\phi \leq 1$, allowing g_T^q to vary in the lattice QCD ranges, we arrive at $d_n < 4 \times 10^{-28} e$ cm [43]. Therefore, observation of the neutron EDM between the current limit of $3 \times 10^{-26} e$ cm [33] and $4 \times 10^{-28} e$ cm would falsify the split-SUSY scenario with gaugino mass unification.

We thank the MILC Collaboration for providing the

2+1+1 flavor HISQ lattices used in our calculations. Simulations were carried out on computer facilities of (i) the USQCD Collaboration, which are funded by the Office of Science of the U.S. Department of Energy, (ii) the Extreme Science and Engineering Discovery Environment (XSEDE), which is supported by National Science Foundation Grant No. ACI-1053575, (iii) the National Energy Research Scientific Computing Center, a DOE Office of Science User Facility supported by the Office of Science of the U.S. Department of Energy under Contract No. DE-AC02-05CH11231; and (iv) Institutional Computing at Los Alamos National Lab. The calculations used the Chroma software suite [44]. This material is based upon work supported by the U.S. Department of Energy, Office of Science of High Energy Physics under Contract No. DE-KA-1401020 and the LANL LDRD program. The work of H.W.L. was supported by DOE Grant No. DE-FG02-97ER4014. We thank Emanuele Mereghatti, Saul Cohen and Anosh Joseph for extensive discussions.

———————

* tanmoy@lanl.gov
† cirigliano@lanl.gov
‡ rajan@lanl.gov
§ hueywenlin@lbl.gov
¶ boram@lanl.gov

[1] D. Dubbers and M. G. Schmidt, Rev.Mod.Phys. **83**, 1111 (2011), arXiv:1105.3694 [hep-ph].
[2] A. Courtoy, S. Baessler, M. Gonzalez-Alonso, and S. Liuti, (2015), arXiv:1503.06814 [hep-ph].
[3] T. Bhattacharya, V. Cirigliano, S. D. Cohen, A. Filipuzzi, M. Gonzalez-Alonso, *et al.*, Phys.Rev. **D85**, 054512 (2012), arXiv:1110.6448 [hep-ph].
[4] T. Bhattacharya, V. Cirigliano, S. Cohen, R. Gupta, A. Joseph, H.-W. Lin, and B. Yoon, (2015), arXiv:1506.06411 [hep-lat].
[5] E. Follana *et al.* (HPQCD Collaboration, UKQCD Collaboration), Phys.Rev. **D75**, 054502 (2007), arXiv:hep-lat/0610092 [hep-lat].
[6] A. Bazavov *et al.* (MILC Collaboration), Phys.Rev. **D87**, 054505 (2013), arXiv:1212.4768 [hep-lat].
[7] A. Hasenfratz and F. Knechtli, Phys.Rev. **D64**, 034504 (2001), arXiv:hep-lat/0103029 [hep-lat].
[8] T. Bhattacharya, S. D. Cohen, R. Gupta, A. Joseph, H.-W. Lin, *et al.*, Phys.Rev. **D89**, 094502 (2014), arXiv:1306.5435 [hep-lat].
[9] S. Collins, G. Bali, and A. Schafer, PoS **LAT2007**, 141 (2007), arXiv:0709.3217 [hep-lat].
[10] G. S. Bali, S. Collins, and A. Schafer, Comput.Phys.Commun. **181**, 1570 (2010), arXiv:0910.3970 [hep-lat].
[11] C. Thron, S. Dong, K. Liu, and H. Ying, Phys.Rev. **D57**, 1642 (1998), arXiv:hep-lat/9707001 [hep-lat].
[12] C. Michael, M. Foster, and C. McNeile (UKQCD collaboration), Nucl.Phys.Proc.Suppl. **83**, 185 (2000), arXiv:hep-lat/9909036 [hep-lat].
[13] T. Blum, T. Izubuchi, and E. Shintani, Phys.Rev. **D88**, 094503 (2013), arXiv:1208.4349 [hep-lat].
[14] A. Abdel-Rehim, C. Alexandrou, M. Constantinou, V. Drach, K. Hadjiyiannakou, *et al.*, Phys.Rev. **D89**, 034501 (2014), arXiv:1310.6339 [hep-lat].
[15] G. Martinelli, C. Pittori, C. T. Sachrajda, M. Testa, and A. Vladikas, Nucl.Phys. **B445**, 81 (1995), arXiv:hep-lat/9411010 [hep-lat].
[16] C. Sturm, Y. Aoki, N. Christ, T. Izubuchi, C. Sachrajda, *et al.*, Phys.Rev. **D80**, 014501 (2009), arXiv:0901.2599 [hep-ph].
[17] In [4] we follow the usual convention of defining the charges for the proton which are related to the neutron charges by the $u \leftrightarrow d$ interchange.
[18] J. de Vries, R. Timmermans, E. Mereghetti, and U. van Kolck, Phys.Lett. **B695**, 268 (2011), arXiv:1006.2304 [hep-ph].
[19] S. Syritsyn, PoS **LATTICE2013**, 009 (2014), arXiv:1403.4686 [hep-lat].
[20] M. Constantinou, PoS **LATTICE2014**, 001 (2014), arXiv:1411.0078 [hep-lat].
[21] J. Green, J. Negele, A. Pochinsky, S. Syritsyn, M. Engelhardt, *et al.*, Phys.Rev. **D86**, 114509 (2012), arXiv:1206.4527 [hep-lat].
[22] G. S. Bali, S. Collins, B. Glssle, M. Gckeler, J. Najjar, *et al.*, Phys.Rev. **D91**, 054501 (2015), arXiv:1412.7336 [hep-lat].
[23] J. Engel, M. J. Ramsey-Musolf, and U. van Kolck, Prog.Part.Nucl.Phys. **71**, 21 (2013), arXiv:1303.2371 [nucl-th].
[24] M. Pospelov and A. Ritz, Annals Phys. **318**, 119 (2005), arXiv:hep-ph/0504231 [hep-ph].
[25] J. R. Ellis and R. A. Flores, Phys. Lett. **B377**, 83 (1996), arXiv:hep-ph/9602211 [hep-ph].
[26] T. Bhattacharya, V. Cirigliano, and R. Gupta, *Proceedings, 30th International Symposium on Lattice Field Theory (Lattice 2012)*, PoS **LATTICE2012**, 179 (2012), arXiv:1212.4918.
[27] M. Pospelov and A. Ritz, Phys.Rev. **D63**, 073015 (2001), arXiv:hep-ph/0010037 [hep-ph].
[28] M. Pitschmann, C.-Y. Seng, C. D. Roberts, and S. M. Schmidt, Phys.Rev. **D91**, 074004 (2015), arXiv:1411.2052 [nucl-th].
[29] A. Bacchetta, A. Courtoy, and M. Radici, JHEP **1303**, 119 (2013), arXiv:1212.3568 [hep-ph].
[30] M. Anselmino, M. Boglione, U. D'Alesio, S. Melis, F. Murgia, *et al.*, Phys.Rev. **D87**, 094019 (2013), arXiv:1303.3822 [hep-ph].
[31] Z.-B. Kang, A. Prokudin, P. Sun, and F. Yuan, Phys.Rev. **D91**, 071501 (2015), arXiv:1410.4877 [hep-ph].
[32] Z.-B. Kang, A. Prokudin, P. Sun, and F. Yuan, (2015), arXiv:1505.05589 [hep-ph].
[33] C. Baker, D. Doyle, P. Geltenbort, K. Green, M. van der Grinten, *et al.*, Phys.Rev.Lett. **97**, 131801 (2006), arXiv:hep-ex/0602020 [hep-ex].
[34] In deriving the bounds, we neglect a possible contribution of the strong CP violating phase Θ. Such a contribution is absent in the Peccei-Quinn scenario [45].
[35] N. Arkani-Hamed and S. Dimopoulos, JHEP **0506**, 073 (2005), arXiv:hep-th/0405159 [hep-th].
[36] G. Giudice and A. Romanino, Nucl.Phys. **B699**, 65 (2004), arXiv:hep-ph/0406088 [hep-ph].
[37] N. Arkani-Hamed, S. Dimopoulos, G. Giudice, and A. Romanino, Nucl.Phys. **B709**, 3 (2005), arXiv:hep-ph/0409232 [hep-ph].

[38] G. Giudice and A. Romanino, Phys.Lett. **B634**, 307 (2006), arXiv:hep-ph/0510197 [hep-ph].

[39] Y. Li, S. Profumo, and M. Ramsey-Musolf, Phys.Rev. **D78**, 075009 (2008), arXiv:0806.2693 [hep-ph].

[40] J. Baron *et al.* (ACME), Science **343**, 269 (2014), arXiv:1310.7534 [physics.atom-ph].

[41] K. Olive *et al.* (Particle Data Group), Chin.Phys. **C38**, 090001 (2014).

[42] S. Abel and O. Lebedev, JHEP **0601**, 133 (2006), arXiv:hep-ph/0508135 [hep-ph].

[43] Note that with QCDSR matrix elements, the split-SUSY upper bound would be less stringent, namely $d_n < 1.2 \times 10^{-27}\, e$ cm.

[44] R. G. Edwards and B. Joo (SciDAC Collaboration, LHPC Collaboration, UKQCD Collaboration), Nucl.Phys.Proc.Suppl. **140**, 832 (2005), arXiv:hep-lat/0409003 [hep-lat].

[45] R. Peccei and H. R. Quinn, Phys.Rev.Lett. **38**, 1440 (1977).